**Proceedings of ASME Turbo Expo 2012**
**GT2012**
**June 11-15, 2012, Copenhagen, Denmark**

# GT2012-68687

# INVESTIGATION OF THE LAMINAR SEPARATION-INDUCED TRANSITION WITH THE $\gamma$-$\widetilde{Re}_{\theta t}$ TRANSITION MODEL ON LOW-PRESSURE TURBINE ROTOR BLADES AT STEADY CONDITIONS

**Jayson Babajee**
Turbomachinery & Propulsion Department
von Karman Institute for Fluid Dynamics
1640 Rhode-Saint-Genèse, Belgium
Email: jayson.babajee@vki.ac.be

**Tony Arts**
Turbomachinery & Propulsion Department
von Karman Institute for Fluid Dynamics
1640 Rhode-Saint-Genèse, Belgium
Email: arts@vki.ac.be

## ABSTRACT

The present study focuses on the assessment and the validation of the Langtry and Menter $\gamma$-$\widetilde{Re}_{\theta t}$ correlation-based transition model, recently implemented in the RANS code elsA from ONERA. The test cases are two Low-Pressure Turbine (LPT) rotor blades, with the same compressible Zweifel loading coefficient but different load distributions. The corresponding experimental results are provided by the von Karman Institute. The outlet isentropic Reynolds number, based on blade chord and outlet isentropic velocity, ranges from 60000 to 250000 in order to investigate the complex separation-induced transition phenomenon occurring at low Reynolds number cruise condition. The turbulence intensity is the natural freestream turbulence of the facility (0.9%). The numerical test campaign gives good predictions, particularly when accurately tailoring the trailing edge and wake regions of the mesh. The numerical mass-averaged kinetic losses are in good agreement with the experimental ones. Moreover, the flow topology parameters (the transition onset, the transition end and the separation) show good agreement in comparison to the experimental results and correlations from the open literature. One is even able to detect separation-induced transition with reattachment before the trailing edge at the lowest Reynolds number. However, the authors stress the turbulence Reynolds number effect on the prediction of separation-induced transition for strong diffusion LPT blades and particularly when the flow is subjected to a long bubble or even an open separation.

## NOMENCLATURE

| | |
|---|---|
| *Acronyms* | |
| AGS | Abu-Ghannam and Shaw transition criterion |
| HL | High-Lift |
| H&W | Hatman and Wang |
| LPT | Low-Pressure Turbine |
| RANS | Reynolds-Averaged Navier-Stokes |
| TD | Extrapolated "S1" decay of turbulence |
| *Symbols* | |
| $c$ | Chord |
| $E$ | Destruction term of transport equation |
| $g$ | Pitch |
| $H$ | Shape factor |
| $k$ | Turbulent kinetic energy |
| $k_l$ | Laminar kinetic energy |
| $l.e.$ / $LE$ | Leading edge |
| $M$ | Mach number |
| $P$ | Production term of transport equation |
| $P_0$ | Total Pressure |
| $R$ | Radius |
| $Re$ | Reynolds number |
| $Re_t$ | Turbulence Reynolds number |
| $Re_v$ | Vorticity Reynolds number |
| $Re_\theta$ | Momentum thickness Reynolds number |
| $Re_{\theta c}$ | Critical momentum thickness Reynolds number |
| $Re_{\theta t}$ | Transition onset momentum thickness Reynolds number |

| | |
|---|---|
| $\widetilde{Re}_{\theta t}$ | Local transition onset momentum thickness Reynolds number (transported variable) |
| $s$ | Curvilinear abscissa |
| $s_0$ | Suction side TE curvilinear abscissa |
| $t$ | Time |
| $T$ | Period |
| $t.e.$ / $TE$ | Trailing edge |
| $Tu$ | Turbulence intensity [in %] |
| $U$ / $V$ | Velocity |
| $x$ | Axial coordinate |
| $y$ | Wall distance |

*Greek symbols*

| | |
|---|---|
| $\beta$ | Flow angle (referred to axial direction) |
| $\gamma$ | Intermittency |
| $\lambda_\theta$ | Pressure gradient parameter |
| $\mu$ | Molecular viscosity |
| $\mu_t$ | Turbulent eddy viscosity |
| $\theta$ | Momentum thickness |
| $\rho$ | Density |
| $\sigma_f$ | $\gamma$-transport equation diffusion coefficient |
| $\sigma_{\theta t}$ | $\widetilde{Re}_{\theta t}$-transport equation diffusion coefficient |
| $\tau_{wall}$ | Wall shear stress |
| $\omega$ | Specific turbulence dissipation rate |
| $\Omega$ | Rotational speed |
| $\Psi$ | Compressible Zweifel loading coefficient |
| $\zeta$ | Mass-averaged kinetic losses [in %] |
| $\Delta H$ | Total enthalpy variation across the rotor blade |
| $\Delta V_\theta$ | Tangential velocity variation across the rotor blade |

*Subscripts*

| | |
|---|---|
| $ax$ | Axial |
| $eff$ | Effective |
| $end$ | End of transition |
| $is$ | Isentropic |
| $sep$ | Separation |
| $onset$ | Onset of transition |
| $\gamma$ | Intermittency |
| $\theta t$ | Momentum thickness at transition onset |
| 1 | Inlet condition |
| 2 | Outlet condition |

## INTRODUCTION

The main topic of this study is to analyze the laminar to turbulent transition mechanisms that occur in a LPT. For this purpose, one can evaluate the work done on the rotor with the turning of the flow from the Euler's momentum equation in a pure axial machine:

$$\Delta H = \Omega \cdot R \cdot \Delta V_\theta \quad (1)$$

A standard LPT is usually made of several stages (4 stages in the case of the CFM56-7B). LPTs commonly operate at an outlet Mach number in the range of 0.6 to 0.9 and weight 20% to 30% of the overall mass of the engine [1]. Thus, the aim is not to manufacture more powerful and heavy aero-engines such as an industrial gas turbine but to get the most efficient one in terms of power with respect to weight and losses mainly. At a first sight, one solution is inevitably to reduce the weight of the LPT by reducing the number of blades. This implies an increase of the pitch-to-chord ratio (g/c). In the meantime, this entails a more important loading per blade in order to compensate for the lower number of working blades for a given stage loading. As a consequence, the velocity suction peak will be higher as well as the diffusion over the rear part of the suction side. Nevertheless, one has to be aware, for this study, of the separation and transition phenomena. This conveys the importance of the Reynolds number (Re) since the current LPT operating Reynolds number is below 100000 at cruise conditions and more than 400000 at take-off. This shows the wide operating conditions of a LPT and above all the changing flow conditions as highlighted by Hourmouziadis [2]. That is why the study of the transition mechanisms is of interest because in the case of open separation, the flow topology is not as the one predicted by standard ideal model.

Therefore, the main aim of this work will be to assess the $\gamma$-$\widetilde{Re}_{\theta t}$ transition model of Langtry and Menter [3] on two HL-LPT rotor blades (where "HL" stands for "High-Lift" and is mainly characterized by the tendency to decrease the number of blades per row and consequently to increase the loading per blade).

## TRANSITION AND SEPARATION PHENOMENA IN LPT

Transition occurs due to the amplification of instabilities in the boundary layer. The main factors to consider are the Reynolds number, the turbulence intensity, the turbulence scales and the pressure gradient.

### Steady Transition

Even though a LPT environment is rather unsteady, one still needs to define the fundamental physics behind steady transition since most of cascade investigations in wind tunnels are carried out at steady condition. There are four kinds of transition. The natural transition, the by-pass transition, the separation-induced transition and the reverse transition (relaminarization).

In LPT cases, the last three cases are of interest since natural transition only occurs at very low turbulence level (below 0.1%). In the by-pass transition, the transition occurs due to disturbances that lead directly to the formation of turbulent spots by by-passing the growth of Tollmien-Schlichting waves. Basically, those disturbances are characterized by a high turbulence level. In the separation-induced transition, the flow is subjected to a separation bubble which is mainly caused by an adverse pressure

gradient and depending on the Reynolds number as well. Then, at low Reynolds numbers and with a strong diffusion (which is the case of HL-LPT), the laminar boundary layer separates and the transition process occurs in the free shear layer. However, depending on the turbulence intensity and scales, the reattachment process may not happen, leading to an open separation which is the worst case in terms of losses. There are three separated flow modes according to the work of Hatman and Wang [4]. Those are the transitional separation mode, the laminar separation/short bubble mode and the laminar separation/long bubble mode. At last, the reverse transition is typically a way back from a turbulent flow to a laminar one which occurs in region of very strong acceleration like along the rear part of the blade pressure side.

### Multimode Transition

This type of transition is an unsteady phenomenon. It is a realistic illustration of the turbomachinery environment where the wakes from a blade row impinge on the following blade row while triggering the transition or inhibiting separation. Actually, the growth of turbulent spots, after the impingement of a wake on the suction side of a blade, implies the apparition of a calmed region which is less sensible to disturbances. They present the advantages of the laminar and turbulent regions without their respective drawbacks [5]. The effectiveness of this calmed region was illustrated in [6, 7]. This region follows the turbulent region at a lower velocity as shown in the work of Schubauer and Klebanoff [8]. They highlighted that the flow starts to be very stable and no breakdown seems to occur from the spot tail. Moreover, the interest of this calmed region is seen in the distance-time diagram (Fig. 1). The difference between the leading and trailing edge velocities of this region insures the development of a laminar look-alike region.

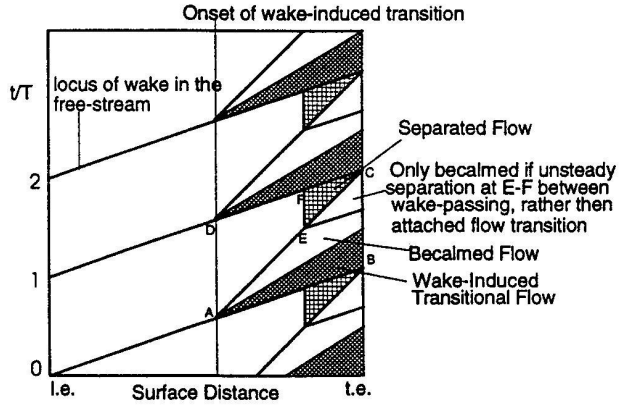


**FIGURE 1. Time-space diagram of the turbulent spots (Schulte and Hodson [9])**

### Parameters Affecting Transition and Separation

At this point of the review, the most important factors affecting transition are the Reynolds number, the turbulence scales, the pressure gradient and the unsteady features of the incoming wakes. However, Mayle [10] depicted the existence of other factors which are less significant in terms of turbulent spot production rate than the pressure gradient such as the surface roughness. Moreover, other designs [11–14] might be of interest such as transversal roughness elements, jets and plasma actuators.

## NUMERICAL APPROACH

To understand the phenomenon of separated-flow transition, one should get a large database in order to assess the findings on each configuration in the aim of making a universal model. However, it could demand a lot of effort since each configuration may be one of a kind and consequently will not infer the principle of universality. That is why data-driven correlations are still useful in predicting models based on trends. The cornerstone of those correlations is the momentum thickness Reynolds number ($Re_\theta$). It is based on the momentum thickness ($\theta$) which quantifies the portion of momentum flux loss due to the presence of the wall. It means that the momentum thickness will behave differently according to the nature of the flow in the boundary layer. That might be an explanation for the perpetual use of this parameter in the correlations. However, one drawback is its complicated assessment in a cascade configuration. Then, one sees the interest of the numerical approach to get more information about this critical parameter.

### Transition Modeling

Most of the transition criteria are based upon empirical correlations [10, 15]. Those criteria are made non-local as they take into account the history of the boundary layer with the freestream information (turbulence intensity and pressure gradient). When the transition criterion is met, the so-called "intermittency weighting function" is switched on from 0 to 1 (like a step) and consequently triggers the production of the turbulent kinetic energy. However, despite its numerical definition, it still keeps the same qualitative meaning of the intermittency coefficient which is the fraction of time during transition for which the flow is turbulent. Besides, this kind of methodology implies the need for the boundary layer thickness calculation from the integration of the velocity profiles. Instead of triggering transition by a switch (via the intermittency weighting function), the transition process should be handle locally with a gradually evolving intermittency weighting function. That is why new methods for the computation of transition founded on transport equations (using local quantities) are of interest such as the $\gamma$-$\widetilde{Re}_{\theta t}$ model of Langtry and Menter [3]. Another transport equation transition model based on the laminar kinetic energy approach [16, 17]

seems promising.

### Correlation-Based Transport Equation Model

The $\gamma$-$\widetilde{Re}_{\theta t}$ model central idea is the van Driest and Blumer's vorticity Reynolds number concept [18]. It allows to link the transition onset momentum thickness Reynolds number to the local boundary layer quantities. The concept is depicted in Eqns. 2 and 3.

$$Re_v = \frac{\rho \cdot y^2}{\mu} \cdot \left| \frac{\partial u}{\partial y} \right| \tag{2}$$

$$Re_\theta = \frac{\max(Re_v)}{2.193} \tag{3}$$

In fact, this model gets rid of the integration of the boundary layer velocity profile along "computation lines" based on the wall mesh lines. Those velocity profiles were used to determine the onset of transition according to non-local transition criteria (such as the Abu-Ghannam and Shaw correlation [15]) in the sense that they are based on the turbulence intensity and the pressure gradient parameter estimated at the edge of the boundary layer.

The transport equation for the numerical intermittency ($\gamma$) is:

$$\frac{\partial(\rho\gamma)}{\partial t} + \frac{\partial(\rho U_j \gamma)}{\partial x_j} = P_\gamma - E_\gamma + \frac{\partial}{\partial x_j}\left[\left(\mu + \frac{\mu_t}{\sigma_f}\right)\frac{\partial \gamma}{\partial x_j}\right] \tag{4}$$

In their first publications, Menter et al. [19] did not disclose all their functions and particularly the $F_{length}$ and the $Re_{\theta c}$ functions. At this time, it was known they were function of the transition onset momentum thickness Reynolds number ($\widetilde{Re}_{\theta t}$). That is why several groups throughout the world focused on the determination of these functions [20–23]. At last, the originators of this transition model published these missing functions [3]. However, in this study, the CFD code elsA relies on the calibrations of those functions performed by Content and Houdeville [23].

The transport equation for the transition onset momentum thickness Reynolds number ($\widetilde{Re}_{\theta t}$) is:

$$\frac{\partial\left(\rho\widetilde{Re}_{\theta t}\right)}{\partial t} + \frac{\partial\left(\rho U_j \widetilde{Re}_{\theta t}\right)}{\partial x_j} = P_{\theta t} + \frac{\partial}{\partial x_j}\left[\sigma_{\theta t}(\mu + \mu_t)\frac{\partial \widetilde{Re}_{\theta t}}{\partial x_j}\right] \tag{5}$$

The purpose of this equation is to transform the non-local empirical correlation into a local quantity in order to compute the transition length function ($F_{length}$) and the critical momentum thickness Reynolds number ($Re_{\theta c}$), necessary for the numerical intermittency equation (Eqn. 4).

Then, when $Re_\theta$ (cf. Eqn. 3) exceeds locally $Re_{\theta c}$ (which is a function of $\widetilde{Re}_{\theta t}$), $\gamma$ equals one due to the activation of the $P_\gamma$ in Eqn. 4. After, a function defines the effective intermittency $\gamma_{eff}$ by the maximum value between $\gamma$ and $\gamma_{sep}$. This latter separation intermittency coefficient ($\gamma_{sep}$) is part of a separation-induced transition correction that allows the local intermittency to exceed one. At last, $\gamma_{eff}$ imposes the laminar regions locally and triggers the transition mechanism by turning on the production term of the turbulent kinetic energy transport equation because this transition model is coupled to the SST $k$-$\omega$ turbulence model. Besides, $\gamma_{eff}$ affects the destruction term of the turbulent kinetic energy transport equation. The mentioned separation-induced transition correction is to let $k$ to grow more rapidly once the boundary layer separates. This is the reason why it exceeds one.

### Phenomenological Transport Equation Model

This laminar kinetic energy ($k_l$) model is based on the laminar fluctuation energy in the pre-transition region of the boundary layer as first introduced by Mayle and Schulz [24]. Their starting point was the fact that the laminar fluctuations preceding transition are primarily caused by the work of the imposed fluctuating free-stream pressure forces on the flow in the boundary layer. This framework has led several research groups to focus on this concept [16, 17]. Lardeau et al. [17] highlighted that the pre-transitional fluctuations leading to bypass transition are due to the presence of low-frequency/low amplitude streamwise vortices in the boundary layer. It turned out that the kinetic energy of the laminar fluctuations ($k_l$) can be described by a transport equation similar to the transport equation for the turbulent kinetic energy ($k$). The objective is to model the pre-transitional fluctuations with the $k_l$ equation. Once a parameter including the kinetic energy is greater than some threshold level, the energy from the streamwise fluctuations $k_l$ is transferred to the turbulent fluctuations [25]. Besides, the transition process is defined by a transfer of energy from $k_l$ to $k$ via the pressure-strain mechanism [16]. It is called "energy redistribution".

## RESULTS

In this section, the investigations of two HL-LPT rotor blades (T108 and T106C) are presented in terms of numerical methodology, comparison with experimental results and assessment of the $\gamma$-$\widetilde{Re}_{\theta t}$ model. The linear cascade configuration as well as the wind tunnel facility are documented in Michálek et al. [26]. The main characteristics of the blades are provided in Tab. 1.

**TABLE 1. Blades Characteristics**

| Blade | T108 | T106C |
|---|---|---|
| $c$ (mm) | 98.42 | 93.01 |
| $c_{ax}$ (mm) | 81.23 | 79.97 |
| Pitch-to-chord ratio, $g/c$ | 0.90 | 0.95 |
| $\beta_1$ (deg) | 33.2 | 33.2 |
| $\Psi=2\cdot\frac{g}{c_{ax}}\cdot\frac{\lvert\rho V_\theta V_x\rvert_2-\lvert\rho V_\theta V_x\rvert_1}{\rho_2 V_2^2}$ | 1.22 | 1.24 |
| Configuration | Front-loaded | Aft-loaded |
| Diffusion Rate, $D_R$ $D_R=\frac{\frac{V_{peak}-V_{2,is}}{V_{2,is}}}{\left\lvert\frac{s_{peak}-s_0}{s_0}\right\rvert}$ | 0.41 | 0.58 |
| Velocity Ratio, $\frac{V_{peak}}{V_{2,is}}$ | 1.31 | 1.30 |
| $M_{2,is}$ | $\{0.5\ ;\ 0.6\}$ | 0.65 |
| $Re_{2,is}$ $(\times 10^3)$ | [60 ; 160] | [80 ; 250] |
| $Tu_{l.e.}(\%)=100\cdot\frac{\sqrt{\frac{2}{3}\cdot k}}{U}$ | 0.9 | 0.9 |
| $Re_t=\frac{\rho k}{\mu\omega}$ | [4.8 ; 12.7] | [6.7 ; 22.2] |

## Computational Methodology

For this approach, three-dimensional CFD simulations are carried out with the in-house ONERA code elsA (ensemble logiciel de simulation en Aérodynamique). The elsA software package is based on a cell-centered finite volume method for solving the Navier-Stokes equations. The space discretization relies on multi-block structured meshes. It allows the simulation of steady or unsteady flows, of inviscid or viscous fluids, in fixed or moving frames. However, in this study, only RANS simulations with the Menter $k$-$\omega$ SST turbulence model are considered, coupled with the $\gamma$-$\widetilde{Re}_{\theta t}$ transition model. The use of the particular single-step case of the Runge-Kutta method for time integration, known as the "Backward Euler" time integration scheme is used. This scheme is coupled with a LU implicit phase technique. The space discretization scheme is a second order Roe scheme. The mesh topology is a periodic standard O4H with High Staggered corrections since the geometries are defined by high values of deviation (Fig. 2). The central O-mesh is around the blade and

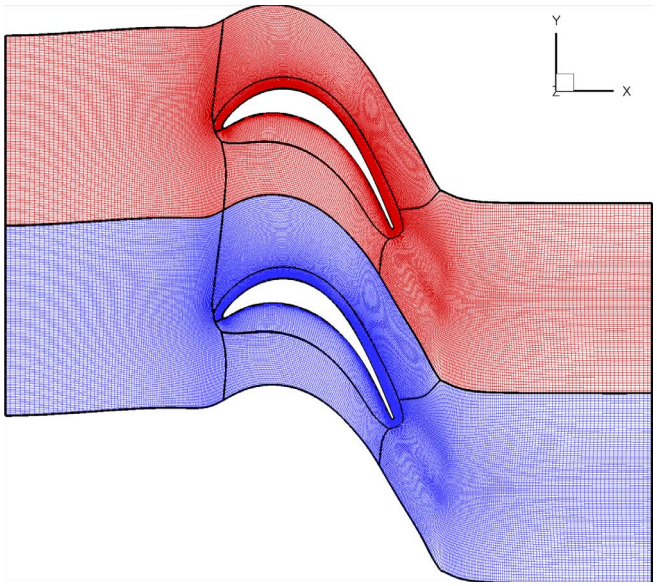


**FIGURE 2. Mesh topology of T106C ($\Psi$=1.24)**

has at least 41 points in the perpendicular direction away from the blade surface. In the streamwise direction around the blade, the number of nodes is above 225 in order to get a good discretization of the suction side of the blade. The extension of the mesh in the spanwise direction is restricted to 5 layers and consequently symmetry boundary conditions are used to define the pseudo-hub and -shroud. This saves a lot of computation time by focusing on the middle of the blade in order to apply convergence acceleration methodologies. As the study focuses on LPT blades which have high aspect-ratios, it is possible to avoid the calculation of the endwall regions. This is to mimic the experimental configuration where the measurements were taken at midspan. This methodology is referred as "2.5D". Thus, the aforementioned steady RANS "2.5D" $\gamma$-$\widetilde{Re}_{\theta t}$ model methodology is meant to be a prediction tool which could be used with an industrial prospect for blade design.

Before starting these test campaigns, a study of the mesh (not presented here for a lack of space) was carried out in order to assess the influence of the wake treatment. It turned out that the wake prediction could be too wide and not deep enough with respect to the experimental wakes (and consequently the mass-averaged kinetic losses). In fact, the cells downstream of the trailing edge of the blade should follow the flow direction. From this mesh strategy, the number of nodes for both configuration is 46605 in one streamwise layer. Moreover, $y^+$ values are below 1

through the Reynolds number ranges.

Concerning the computational inlet conditions for distant boundaries, one needs to provide turbulence and transition variables. About the transition ones, $\gamma$ is set to 1.0 and $\widetilde{Re}_{\theta t}$ is determined by a correlation [3]. The turbulence variables (turbulent kinetic energy $k$ and specific turbulence dissipation rate $\omega$), at those inlet conditions, are incompletely known according to Spalart and Rumsey [27]. However, the decay of turbulence, ahead of the cascade, is available from the test campaign carried out at the von Karman Institute [26] where it was assessed behind a turbulence grid in the S1 facility. This "S1" decay law was compared to a decay law from Chassaing [28]. He described two phases of the decay of turbulence. The initial phase is defined as the prevalence of the eddies in the decay of turbulence (in the region downstream the turbulence grid). The final phase is defined as the prevalence of the dissipation in the decay of turbulence (far downstream the turbulence grid). In Fig. 3, one can see the good agreement between the two sets of decay of turbulence (the "S1" one and the initial phase one from Chassaing [28]). Then, since the turbulence intensity measured without any grid of turbulence (0.9%) is in between the initial and final phases but closer to the initial phase, an extrapolation of the "S1" decay law was done in order to get the input values (and particularly the dissipation rate) for the inlet boundary conditions. Thus, from this extrapolated "S1" decay law, it is possible to set the inlet boundary conditions according to the desired values at the leading edge plane. When assessing the CFD predictions of the turbulence evolution ahead of the cascade at several outlet isentropic Reynolds number ($Re_{2,is}$), one can see that the inlet boundary condition inputs enable the CFD predictions to match the experimental trends (Fig. 3). Then, this methodology for imposing the dissipation rate at the inlet boundary condition is adopted for this study. To give an order of magnitude, the Kolmogorov length scale for the T106C blade at $Re_{2,is} = 120000$, $M_{2,is} = 0.65$ and $Tu_{l.e.} = 0.9\%$ is $4.10^{-4}$ m for the CFD calculation whereas Michalek et al. [2010], who carried out the experimental investigation of this configuration, had $5.10^{-4}$ m.

Finally, a comparison between the well-used non-local transition criterion of Abu-Ghannam and Shaw (AGS) [15] and the newly implemented transition transport equation model $\gamma$-$\widetilde{Re}_{\theta t}$ [3] was carried out in order to show the superiority of this transport equation model since both approaches are correlation-based but differ from the way the information is treated (non-locally or locally). Figure 4 shows this superiority with the isentropic Mach number ($M_{is}$) distribution along the suction side of the T108 blade. Besides, it has to be reminded that the correlation of Abu-Ghannam and Shaw [15], which is part of the framework behind the correlation used in Langtry and Menter transition model [3], is based upon experimental data which pressure gradient parameter ($\lambda_\theta$) is between $\pm 0.1$. In the current study, the two HL-LPT rotor blades have a $\lambda_\theta$ that can be lower than $-0.1$.

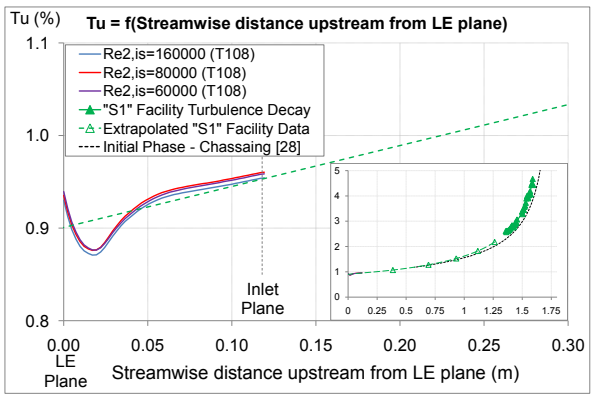


**FIGURE 3. "S1" Decay of turbulence ahead of the cascade**

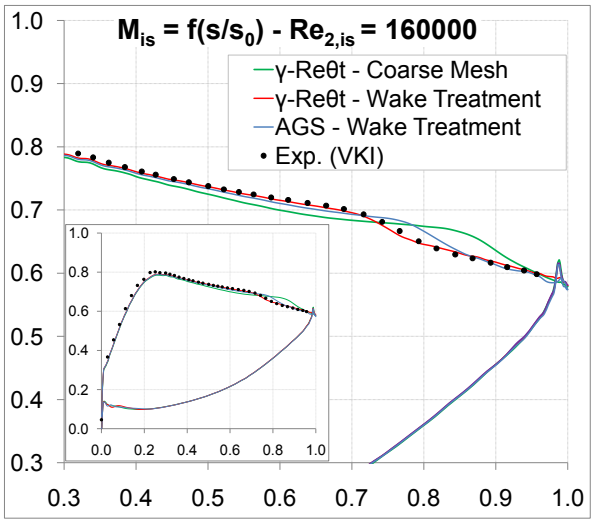


**FIGURE 4. T108 comparison of $\gamma$-$\widetilde{Re}_{\theta t}$ model and AGS criterion at $Re_{2,is} = 160000$, $M_{2,is} = 0.6$ and $Tu_1 = 0.9\%$ (abscissa: $s/s_0$, ordinate: $M_{is}$)**

## T108 Cascade

After setting up the methodologies of the study, one can focus on the T108 blade and the comparison with other research groups using different transition models and/or different methodologies. Corral and Gisbert [29] worked on this geometry with the $\gamma$-$\widetilde{Re}_{\theta t}$ model coupled with the RANS solver $Mu^2s^2T$. Their model features a $\widetilde{Re}_{\theta t}$-transport equation diffusion coefficient ($\sigma_{\theta t}$) equals to 10 and a $s_1$ function (which controls the reattachment location [30]) depending upon $\widetilde{Re}_{\theta t}$ and the distance to the wall. They performed 2D computations with a very fine unstructured mesh of 70000 points. Pacciani et al. [31] used the laminar kinetic energy concept coupled with the Wilcox $k$-$\omega$ turbulence model. They performed 2D computations with a non-periodic single-block O-type mesh of 57521 nodes. Benyahia et al. [32] used the RANS code elsA developed by ONERA. They worked

on the implementation of the $\gamma$-$\widetilde{Re}_{\theta t}$ transition model and used it coupled with the Menter $k$-$\omega$ SST turbulence model. They performed 3D computations with a O4H structured mesh of 14545 points in one spanwise layer. The difference between Benyahia et al. [32] $\gamma$-$\widetilde{Re}_{\theta t}$ model and the one used in the present work is the value of the diffusion coefficient ($\sigma_{\theta t}$=10 in Benyahia et al. [32] and $\sigma_{\theta t}$=2 in the present work, value recommended by Langtry and Menter [3]). At last, the VKI experimental results [33] are provided.

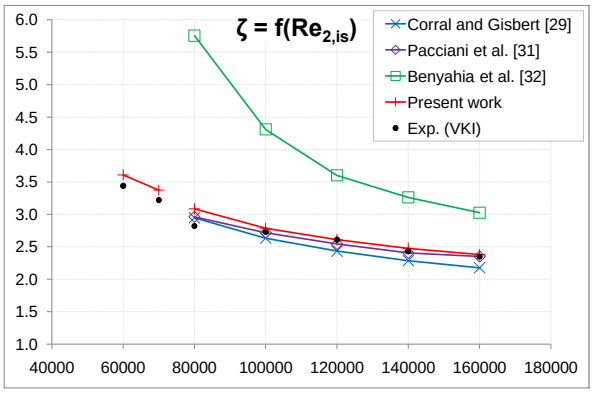


**FIGURE 5. T108 mass-averaged kinetic losses (abscissa: $Re_{2,is}$, ordinate: $\zeta$)**

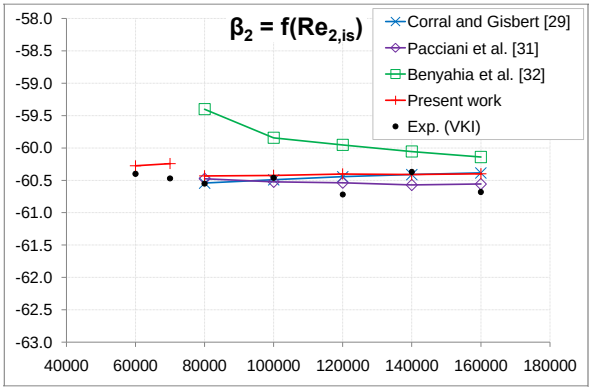


**FIGURE 6. T108 mass-averaged outlet flow angle (abscissa: $Re_{2,is}$, ordinate: $\beta_2$)**

The comparisons, in terms of mass-averaged kinetic losses ($\zeta$) and outlet flow angle ($\beta_2$), are depicted in Figs. 5 and 6. From these figures, one can see that the present study predictions are in good agreement with the experimental measurements over the full $Re_{2,is}$ range. As a remark, the break in the $Re_{2,is}$ range is intentional since the two lowest $Re_{2,is}$ were performed in

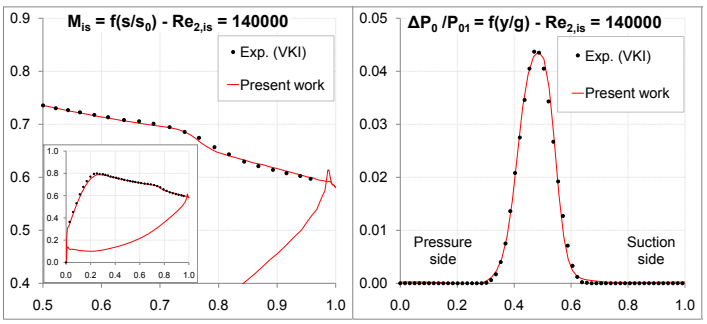


**FIGURE 7. T108 isentropic Mach number distribution and wake profile at $Re_{2,is} = 140000$ (left abscissa: $s/s_0$, left ordinate: $M_{is}$, right abscissa: $y/g$, right ordinate: $\Delta P_0/P_{01}$)**

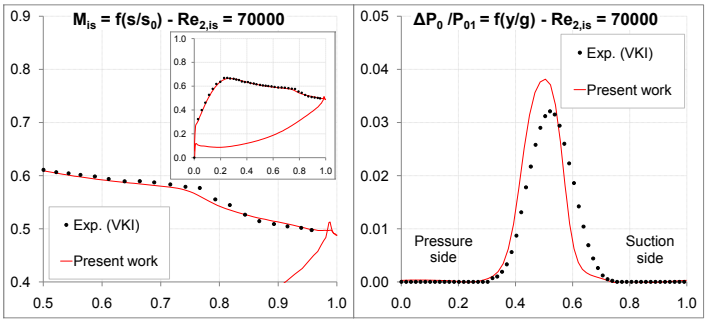


**FIGURE 8. T108 isentropic Mach number distribution and wake profile at $Re_{2,is} = 70000$ (left abscissa: $s/s_0$, left ordinate: $M_{is}$, right abscissa: $y/g$, right ordinate: $\Delta P_{01}/P_{01}$)**

the facility at a lower outlet isentropic Mach number ($M_{2,is}$=0.5 instead of 0.6). From those trends, the similarity between the correlation-based transition model (Corral and Gisbert [29] and the present study) is remarkable even though the calibration parameters are not the same (such as $\sigma_{\theta t}$ and $s_1$). This could be a reason why an offset in the trends is noticeable. However, this might be due to the different values of the turbulence Reynolds number ($Re_t = \mu_t/\mu = (\rho k)/(\mu\omega)$) used between the two groups to compute the dissipation rate at the inlet boundary condition. The quality of the mesh in both studies does not seem to imply any mesh dependency. This last point leads to the comparison between the present study predictions with the ones of Benyahia et al. [32]. Their predictions overestimate the experimental results, even though they got good predictions of the $M_{is}$ distribution over the blade suction side. The reason is a question of mesh dependency since they used the coarsest mesh among all the presented studies and there is no apparent wake treatment or refinement in the wake vicinity. At last, the comparison with Pacciani et al. [31] predictions leads to a good matching. Since their laminar kinetic energy approach is intented to be based on more physical models, one can conclude on the reliability of the correlation-based transition model, used in this study, for this HL-LPT blade

configuration. Moreover, the $M_{is}$ distribution over the suction side of the blade as well as the wake profile, extracted at $0.5 \cdot c_{ax}$ downstream the trailing edge, of two $Re_{2,is}$ (140000 and 70000) are provided (Figs. 7 and 8). From these plots, one can assess the fairly good wake predictions in terms of width and depth. The $M_{is}$ distributions are pretty good as well in terms of pressure plateau, reattachment and Mach number level.

## T106C Cascade

After the results of a front-loaded blade (T108) with a mild diffusion rate (Tab. 1), the study of an aft-loaded blade (T106C) with a strong diffusion is presented below. Like the former section, the same research groups worked on the T106C blade with the same methodology and numerical approach, except Benyahia et al [32] who used for the T106C a finer mesh with a wake treatment. Once again, the comparisons in terms of $\zeta$ and $\beta_2$ are illustrated (Figs. 9 and 10).

This time, the $\zeta$ are well predicted up to $Re_{2,is} = 140000$. For lower values, one can observe the underprediction of the "TD" trend which corresponds to the value extracted from the extrapolated "S1" decay law. Apparently, the values of $Re_t$ used by the other research groups are lower than the one used in the 'TD" trend (Tab. 1). In fact, Pacciani et al. [31] used a ratio of turbulence length scale over the axial chord of $2.5 \times 10^{-3}$ which represents a value of $Re_t$ of approximately 0.93. Benyahia et al. [32] used a value of 0.1. Since the predictions seem to be $Re_t$-dependent, a study of this $Re_t$ was carried out. From Figs. 9 and 10, one can see the improvements of the predictions (particularly at low $Re_{2,is}$) by lowering $Re_t$ (up to 0.01). Concerning the other research groups, they are able to catch the bursting of the bubble (i.e. when the topology of the bubble changes from a short one to a long one and when the pressure distribution is clearly affected [34]) and even an open separation.

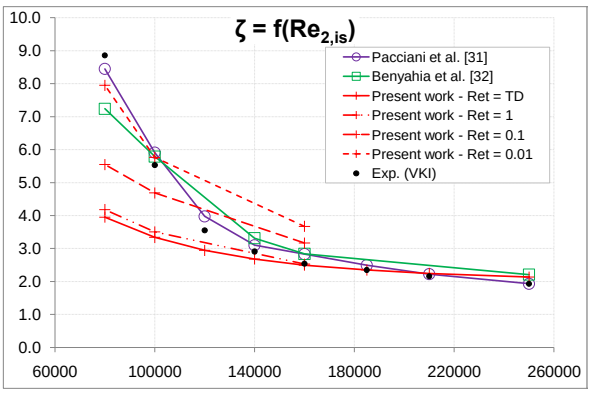


**FIGURE 9. T106C mass-averaged kinetic losses (abscissa: $Re_{2,is}$, ordinate: $\zeta$)**

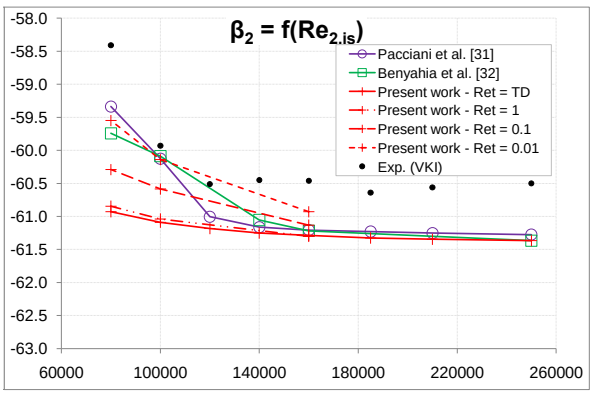


**FIGURE 10. T106C mass-averaged outlet flow angle (abscissa: $Re_{2,is}$, ordinate: $\beta_2$)**

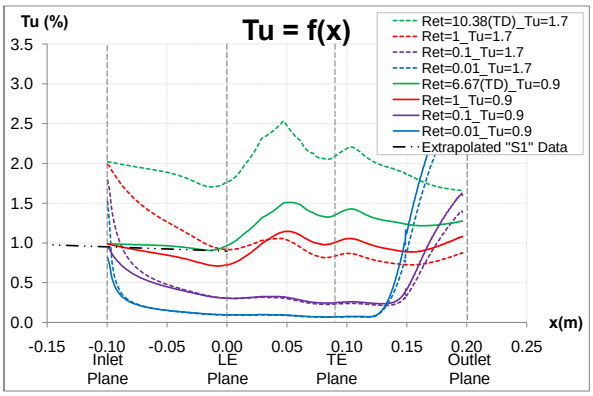


**FIGURE 11. Turbulence across T106C cascade at $Re_{2,is} = 80000$ with the influence of the $Re_t$**

Let's have an insight at the level of turbulence across the cascade in the "freestream" region (between two blades) for $Re_{2,is} = 80000$. From Fig. 11, one can see that for $Re_t = 0.01$, the level of turbulence is really low (around 0.1%). This behavior is close to a pseudo-laminar case or an external flow configuration. Moreover, it does not follow the extrapolated "S1" decay law. This conclusion is applicable to $Re_t = 0.1$ as well whereas $Re_t = 1$ seems close to the extrapolated "S1" decay law. In fact, when checking the $M_{is}$ distribution, one can notice the proximity of the $Re_t = 1$- and $Re_t = TD$-cases (Fig. 12). In addition, from the experimental data, one would expect an open separation. This is predicted by the two lowest $Re_t$ (0.1 and 0.01) where the $M_{is}$ distributions are affected by this open separation phenomenon as illustrated by a lower peak Mach number as well as a more upstream position of it [34]. Morever, it is followed by a longer pressure plateau. In addition, the wake profile (Fig. 12), extracted at $0.5 \cdot c_{ax}$ downstream the trailing edge, illustrates the correct prediction done by the lowest $Re_t$. The wake profile is wider and deeper (which confirms the influence of the open sep-

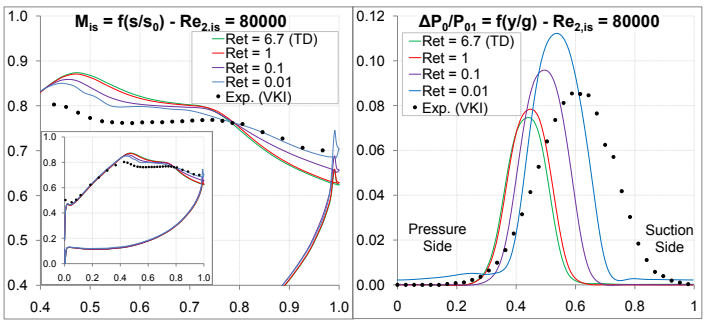


**FIGURE 12. T106C isentropic Mach number distribution and wake profile with $Re_t$ effect at $Re_{2,is} = 80000$ (left abscissa: $s/s_0$, left ordinate: $M_{is}$, right abscissa: $y/g$, right ordinate: $\Delta P_{01}/P_{01}$)**

aration on the size of the boundary layer and consequently the velocity deficit). The investigation of a higher inlet turbulence level (1.7%) illustrates the preponderance of the dissipation at low $Re_t$ on the turbulent kinetic energy level (Fig. 11).

## Validation of the $\gamma$-$\widetilde{Re}_{\theta t}$ Transition Model Implemented in elsA: Assessment of the Flow Topology Parameters

In this last section, a focus on the flow topology parameters is illustrated. These parameters are the transition onset, the transition end and the separation locations. One can extract them from both the numerical and experimental data. However, $Re_\theta$ is only accessible via the numerical data. Then, one can compare those information with correlations of the open literature.

To get those flow topology parameters, one can rely on the effective intermittency ($\gamma_{eff}$), the viscosity ratio ($\mu_t/\mu$), the shape factor ($H$) and the wall shear stress ($\tau_{wall}$). $\gamma_{eff}$ is the output of the correlation behind the transition model. While scanning the boundary layer from the wall to the edge, one can use this parameter when it suddenly increases to 1 and then decreases. The sudden increase might be defined as the transition onset. This position is considered as the moment where the intermittency first start to grow [30]. Besides, there is a correlation between $Re_{\theta c}$ and $\widetilde{Re}_{\theta t}$ which defines the lag between the first rise of intermittency and the moment where the skin friction start to increase [30]. For $\mu_t/\mu$, one can assess the transition onset when it exceeds 1. This criterion is defined by the ratio of the eddy viscosity and the molecular viscosity. Thus, when this ratio exceeds one, it means the turbulence patterns are preponderant. For $H$, one can assess the transition onset when it is maximum before any sudden decrease. Indeed, it is well-known that the shape factor of a laminar boundary layer ($H \approx 2.6$) is higher than a turbulent one ($H \approx 1.3$) in a flat plate configuration. Moreover, the shape factor is influenced by an adverse pressure gradient in those HL-LPT configurations. Thus, it allows to assess the position of a possible separation point when $H$ exceeds 3.5. For $\tau_{wall}$, one will notice a sudden increase of it close to its minimum value. When $\tau_{wall}$ starts to stabilize at a constant value and even to decrease in order to follow the trend of the fully turbulent case, then this position is defined as the transition end. When $\tau_{wall}$ is negative, this indicates a separation. When $\tau_{wall}$ exceeds zero after being negative, one can define a reattachment. About the experimental information, one can assess the flow topology parameters with the combination of the $M_{is}$ distribution over the blade [5] and the pseudo-wall shear stress [26].

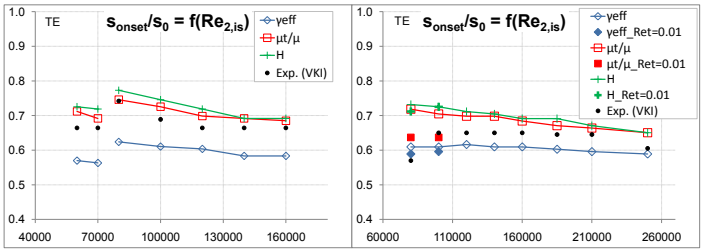


**FIGURE 13. Transition onset through the $Re_{2,is}$ range for T108 (left) and T106C (right) (abscissa: $Re_{2,is}$, ordinate: $s_{onset}/s_0$)**

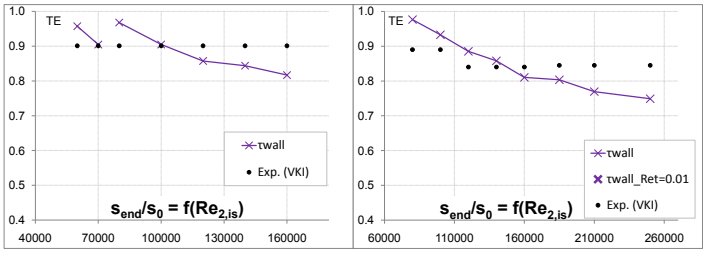


**FIGURE 14. Transition end through the $Re_{2,is}$ range for T108 (left) and T106C (right) (abscissa: $Re_{2,is}$, ordinate: $s_{end}/s_0$)**

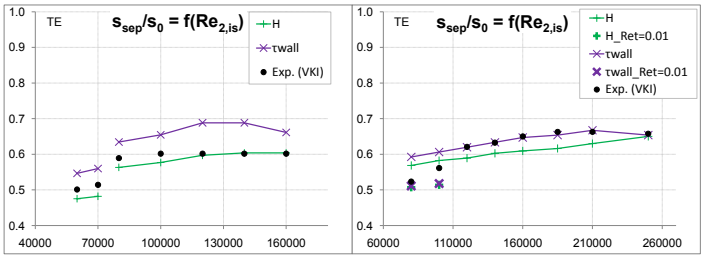


**FIGURE 15. Separation through the $Re_{2,is}$ range for T108 (left) and T106C (right) (abscissa: $Re_{2,is}$, ordinate: $s_{sep}/s_0$)**

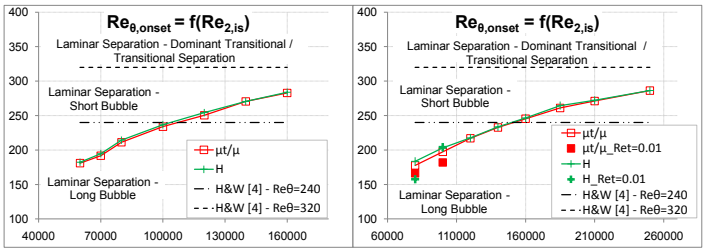


**FIGURE 16**. $Re_{\theta,onset}$ **through the** $Re_{2,is}$ **range for T108 (left) and T106C (right) (abscissa:** $Re_{2,is}$**, ordinate:** $Re_{\theta,onset}$**)**

From Fig. 13, one can see the evolution of the transition onset location with $Re_{2,is}$. For the T108 case, the movement of the transition onset towards the trailing edge as $Re_{2,is}$ decreases is well captured by the flow topology parameters, except $\gamma_{eff}$ which predicts earlier transition onsets. In fact, this was expected since $\gamma_{eff}$ defines the moment when $Re_{\theta c}$ is reached and where $\gamma$ first starts to grow [30]. One can draw the same conclusion about the T106C blade except that at low $Re_{2,is}$, the flow is prone to long bubble and open separation bubble topologies which affect the positions of separation and transition onset significantly [5]. From both the T106C experimental data and numerical predictions, the trend of the transition onset to travel downstream as $Re_{2,is}$ decreases is respected. However, when decreasing more $Re_{2,is}$, the $Re_t$ effect is clearly visible. Thus, the expected upstream movement of the transition onset is not predicted in the extrapolated "S1" decay law $Re_t$-case whereas it is predicted when $Re_t$ is extremely low (0.01, depicted by the plain symbols in Fig. 13). Concerning the separation point (Fig. 15), its upstream movement as $Re_{2,is}$ decreases is respected from both the experimental and numerical data. Once again, the $Re_t$ effect is noticeable in the T106C case. About the transition end position (Fig. 14), its downstream movement as $Re_{2,is}$ decreases is predicted by the numerical approach while it seems pretty constant for the experimental predictions through the $Re_{2,is}$ range. The reason, which is also applicable to the experimental transition onsets, is the low spatial resolution of the pseudo-wall shear stress measurements. There are 15 hot-film gauges, spread over the suction side. They are regularly spaced in the deceleration part ($\sim$5 mm in the curvilinear axis). At last, Fig. 16 illustrates the relationship between the momentum thickness Reynolds number at onset of transition ($Re_{\theta,onset}$) and $Re_{2,is}$ for both blade. In addition to the numerical predictions, the criteria proposed by Hatman and Wang [4] are depicted. As expected, the higher $Re_{2,is}$ are situated in the "Laminar Separation - Short Bubble" region of the plot. Then, the bursting $Re_{2,is}$ for the T108 blade is considered to be around 100000. This is corroborated by $\zeta$ as well as $\beta_2$ trends (Figs. 5 and 6). Likewise, the T106C bursting $Re_{2,is}$ is assessed with Fig. 16 and is considered to be around 140000, which is confirmed by $\zeta$ as well as $\beta_2$ trends (Figs. 9 and 10).

## CONCLUSIONS

A new and promising transport equation transition model [3], recently implemented in elsA [23] (one equation for $\gamma$ and the other one for $\widetilde{Re_{\theta t}}$), was assessed on two HL-LPT rotor blades (T108 and T106C). Since those blades are prone to separation-induced transition, they form a good sample group for the model validation as a prediction tool.

In the present work, the authors focused on the importance of the turbulent variables boundary conditions which are commonly defined by $Re_t$. It was concluded, from the experimental decay law, that one can predict the state of the boundary layer, and consequently $\zeta$ for mild diffusion HL-LPT rotor blades (T108). For more harsh diffusion HL-LPT rotor blades (T106C), the boundary layer state predictions are satisfactory for mid-$Re_{2,is}$ but are underestimated in the low-$Re_{2,is}$ range where long bubble and open separation topologies are encountered. In fact, an investigation of $Re_t$ has illustrated the influence of this parameter on the boundary layer state predictions. Thus, by lowering more and more this parameter, and as a consequence increasing the dissipation rate, it was possible to predict the expected flow topologies. However, this high dissipation rate does not fulfill the requirements of the experimental decay of turbulence as the flow in the cascade is defined by really low levels of turbulence ($\sim$0.1%). Therefore, this low-$Re_t$ approach lacks of predictive behavior as a tuning seems necessary. Nevertheless, an investigation of the diffusion of the turbulent variables into the boundary layer might be of interest in order to understand how it affects the position of separation. Indeed, it seems this position impacts the onset of transition according to the $Re_t$-investigation (the upstream movement of separation point induces an upstream movement of the transition onset at low $Re_{2,is}$ whereas it induces a downstream movement at mid $Re_{2,is}$). Besides, one has to remember the correlation for the onset of transition in the adverse pressure gradient region is basically meant for attached flows [15, 19] and ranges up to $\lambda_\theta = \pm 0.1$ ($\lambda_\theta$ can be lower than $-0.1$ for the HL-LPT blade cases of the present work).

Concerning those flow topology parameters, their assessment reveals to be in good agreement with the experimental results as well as correlations from the literature [4].

At last, this steady RANS approach using this new transition model exhibits its robustness in predicting separation-induced transition for mild diffusion HL-LPT rotor blades but needs to be carefully used if strong diffusion HL-LPT configurations are intended for investigation. In fact, more work on the calibration process is expected in order to extend the applicability of this promising model on strong diffusion HL-LPT blades.

## ACKNOWLEDGMENTS

The experimental results reported in this work were obtained within the European research project TATMo "Turbulence and Transition Modelling for Special Turbomachinery Applications"

(AST5-CT-2006-030939).

The authors would like to thank SNECMA for the permission to publish this article. They are also grateful to Jan Michálek (VKI) and Abdelkader Benyahia (ONERA) for the constructive discussions.

## REFERENCES

[1] Hodson, H. P., and Howell, R. J., 2005. "The Role of Transition in High Lift Low Pressure Turbines". *von Karman Institute for Fluid Dynamics Lecture Series,* ***2005-03***, April 25-29.

[2] Hourmouziadis, J., 1989. "Aerodynamic Design of Low Pressure Turbines". *AGARD Lecture Series,* ***167***.

[3] Langtry, R. B., and Menter, F. R., 2009. "Correlation-Based Transition Modeling for Unstructured Parallelized Computational Fluid Dynamics Codes". *AIAA Journal,* ***47***(12), December, pp. 2894–2906.

[4] Hatman, A., and Wang, T., 1999. "A Prediction Model for Separated-Flow Transition". *ASME Journal of Turbomachinery,* ***121***(3), July, pp. 594–602.

[5] Coton, T., 2003. "Unsteady Wake-Boundary Layer Interaction on Advanced High Lift Low Pressure Turbine Airfoils". PhD thesis, Université Libre de Liège, December.

[6] Pfeil, H., and Herbst, R., 1979. "Transition Procedure of Instationary Boundary Layers". In ASME Gas Turbine Conference and Exhibit and Solar Energy Conference, no. 79-GT-128.

[7] Pfeil, H., Herbst, R., and Schröder, T., 1983. "Investigation of the Laminar-Turbulent Transition of Boundary Layers Disturbed by Wakes". *ASME Journal of Engineering for Power,* ***105***(1), January, pp. 130–137.

[8] Schubauer, G. B., and Klebanoff, P. S., 1955. Contributions on the Mechanics of Boundary-Layer Transition. Technical Note 3489, National Advisory Commitee for Aeronautics, September.

[9] Schulte, V., and Hodson, H. P., 1998. "Prediction of the Becalmed Region for LP Turbine Profile Design". *ASME Journal of Turbomachinery,* ***120***(4), October, pp. 839–846.

[10] Mayle, R. E., 1991. "The Role of Laminar-Turbulent Transition in Gas Turbine Engines". *ASME Journal of Turbomachinery,* ***113***(4), October, pp. 509–537.

[11] Himmel, C. G., and Hodson, H. P., 2009. "Modifying Ultra-High Lift Low Pressure Turbine Blades for Low Reynolds Number Applications". In 12th International Symposium on Unsteady Aerodynamics, Aeroacoustics & Aeroelasticity of Turbomachines (ISUAAAT12), no. I12-S7-3.

[12] Himmel, C. G., and Hodson, H. P., 2009. "Passive Air Jets for Loss Reductions in High Lift Low Pressure Turbines". In ISABE, no. 1295.

[13] Volino, R. J., Kartuzova, O., and Ibrahim, M. B., 2009. "Experimental and Computational Investigations of Low-Pressure Turbine Separation Control Using Vortex Generator Jets". In ASME Turbo Expo 2009: Power for Land, Sea and Air, no. GT2009-59983.

[14] Huang, J., Corke, T. C., and Thomas, F. O., 2006. "Plasma Actuators for Separation Control of Low-Pressure Turbine Blades". *AIAA Journal,* ***44***(1), January, pp. 51–57.

[15] Abu-Ghannam, B. J., and Shaw, R., 1980. "Natural Transition of Boundary Layers - The Effects of Turbulence, Pressure Gradient and Flow History". *Journal Mechanical Engineering Science,* ***22***(5), pp. 213–228.

[16] Walters, D. K., and Cokljat, D., 2008. "A Three-Equation Eddy-Viscosity Model for Reynolds-Averaged Navier-Stokes Simulations of Transitional Flow". *ASME Journal of Fluids Engineering,* ***130***(12), December, pp. 121401.1–121401.14.

[17] Lardeau, S., Li, N., and Leschziner, M. A., 2007. "Large Eddy Simulation of Transitional Boundary Layers at High Free-Stream Turbulence Intensity and Implications for RANS Modeling". *ASME Journal of Turbomachinery,* ***129***(2), April, pp. 311–317.

[18] van Driest, E. R., and Blumer, C. B., 1963. "Boundary Layer Transition: Freestream Turbulence and Pressure Gradient Effects". *AIAA Journal,* ***1***(6), June, pp. 1303–1306.

[19] Menter, F. R., Langtry, R. B., Likki, S. R., Suzen, Y. B., Huang, P. G., and Völker, S., 2006. "A Correlation-Based Transition Model Using Local Variables - Part I: Model Formulation". *ASME Journal of Turbomachinery,* ***128***(3), July, pp. 413–422.

[20] Piotrowski, W., Elsner, W., and Drobniak, S., 2008. "Transition Prediction on Turbine Blade Profile with Intermittency Transport Equation". In ASME Turbo Expo 2008: Power for Land, Sea and Air, no. GT2008-50796.

[21] Malan, P., Suluksna, K., and Juntasaro, E., 2009. "Calibrating the $\gamma$-$Re_\theta$ Transition Model". In ERCOFTAC Bulletin 80, pp. 53–57.

[22] Elsner, W., Piotrowski, W., and Warzecha, P., 2009. "Transition Modelling with Intermittency Transport Equations". In ERCOFTAC Bulletin 80, pp. 49–52.

[23] Content, C., and Houdeville, R., 2010. "Application of the $\gamma$-$R_\theta$ laminar-turbulent transition model in Navier-Stokes computations". In AIAA 40th Fluid Dynamics Conference and Exhibit, no. AIAA 2010-4445.

[24] Mayle, R. E., and Schulz, A., 1997. "The Path to Predicting Bypass Transition". *ASME Journal of Turbomachinery,* ***119***(3), July, pp. 405–411.

[25] Dick, E., 2009. "Eddy Viscosity Models for Turbulence and Transition". *von Karman Institute for Fluid Dynamics Lecture Series,* ***2009-08***, September 21-25.

[26] Michálek, J., Monaldi, M., and Arts, T., 2010. "Aerodynamic Performance of a Very High Lift Low Pressure Turbine Airfoil (T106C) at Low Reynolds and High Mach Number with Effect of Free Stream Turbulence Intensity".

In ASME Turbo Expo 2010: Power for Land, Sea and Air, no. GT2010-22884.

[27] Spalart, P. R., and Rumsey, C. L., 2007. "Effective Inflow Conditions for Turbulence Models in Aerodynamic Calculations". *AIAA Journal,* ***45***(10), October, pp. 2544–2553.

[28] Chassaing, P., 2000. *Turbulence en mécanique des fluides - Analyse du phénomène en vue de sa modélisation à l'usage de l'ingénieur*, 1st ed. Cépaduès-Editions, August.

[29] Corral, R., and Gisbert, F., 2010. "Prediction of Separated-Induced Transition Using a Correlation-Based Transtion Model". In ASME Turbo Expo 2010: Power for Land, Sea and Air, no. GT2010-23239.

[30] Langtry, R. B., 2006. "A Correlation-Based Transition Model using Local Variables for Unstructured Parallelized CFD codes". PhD thesis, Universität Stuttgart, May 31.

[31] Pacciani, R., Marconcini, M., Arnone, A., and Bertini, F., 2010. "A CFD Study of Low Reynolds Number Flow in High Lift Cascades". In ASME Turbo Expo 2010: Power for Land, Sea and Air, no. GT2010-23300.

[32] Benyahia, A., Castillon, L., and Houdeville, R., 2011. "Prediction of Separation-Induced Transition on High Lift Low Pressure Turbine Blade". In ASME Turbo Expo 2011: Power for Land, Sea and Air, no. GT2011-45566.

[33] Michálek, J., Ilikan, A., and Arts, T., 2011. "A Comparison of High and Low Speed Aerodynamic Performance of a Very High Lift Low-Pressure Turbine Airfoil (T108) at Low Reynolds Numbers: Experimental Analysis and Numerical Prediction". In 9th European Conference on Turbomachinery Fluid Dynamics and Thermodynamics.

[34] Roberts, W. B., 1973. "A Study of the Effect of Reynolds number and Laminar Separation Bubbles on the Flow through Axial Compressor Cascades". PhD thesis, Université Libre de Bruxelles, May.